In Situ Quantitative Assessment of the Role of Silicon During the Quenching and Partitioning of a 0.2C Steel

PIERRE HUYGHE, MATTEO CARUSO, JEAN-LOUIS COLLET, SYLVAIN DÉPINOY, and STÉPHANE GODET

Silicon is an essential alloying element added in quenching and partitioning (Q&P) steels to delay and/or suppress carbide precipitation. However, there is a strong industrial interest to reduce the silicon content as it has detrimental effects on the metallurgical route. This work investigates by means of *in situ* high-energy XRD (HEXRD) the effect of silicon on the microstructural evolution during quenching and partitioning of a commercial 0.2C-2.3Mn grade. The results of this study highlight the role of the bainite transformation during the reheating and partitioning steps for effective austenite retention. Silicon influences the kinetics of austenite decomposition into bainite and finally promotes the stabilization of austenite. This is explained by the ability of silicon to suppress carbide precipitation (i) at the interface between bainite and austenite and (ii) in the martensite matrix. Carbide precipitation at the bainite/austenite interface decreases the amount of carbon that diffuses from bainite to austenite, subsequently accelerating the bainite transformation kinetics and preventing austenite stabilization. Carbide precipitation in martensite reduces the amount of carbon available for partitioning in austenite, further preventing its stabilization. Additions of elements such as Cr or Mo could be therefore considered in order to reduce the austenite decomposition in low-silicon steel grades.

https://doi.org/10.1007/s11661-019-05281-2

I. INTRODUCTION

THE quenching and partitioning (Q&P) process was first proposed by Speer *et al.* in 2001 as a heat treatment designed to stabilize austenite in steels at room temperature.[1] It consists of two main steps. The first step after intercritical annealing or full austenitization is an interrupted quench between the martensite-start temperature (M_s) and the martensite-finish temperature (M_f), in order to form a controlled fraction of martensite. This is followed by a partitioning step during which the untransformed austenite is stabilized through carbon partitioning from martensite.[1,2] Q&P steels typically exhibit a good combination of strength and ductility, the latter being due to the transformation of retained austenite upon straining (TRIP effect).[3] The intensity of the TRIP effect depends on the amount and on the stability of the retained austenite, which in turn depends on its carbon content, size, surrounding phases, and stress state.[4–8] To improve austenite stabilization, carbon partitioning from martensite to austenite should be promoted, and consequently, competing mechanisms such as carbide precipitation and austenite decomposition should be suppressed. This is achieved through optimization of the Q&P thermal cycle or optimization of the steel composition.[3,9–11] Silicon is an essential alloying element in Q&P as it delays and/or suppresses the precipitation of carbides in martensite.[12–16] However, there are strong industrial motivations to reduce the silicon content in Q&P steels for automotive applications, since silicon has a detrimental effect on several steps of the industrial process (slab embrittlement, descaling issues, difficult pickling, and poor coatability).[17] It is thus of prime interest to investigate how the silicon influences the microstructural evolution during a Q&P treatment in order to optimize its content in future commercial grades.

The relationship between silicon content, carbide precipitation, and the amount of retained austenite in Q&P steels is not straightforward. The recent literature,

PIERRE HUYGHE, SYLVAIN DÉPINOY, and STÉPHANE GODET are with the 4MAT, Materials Engineering, Characterization, Processing and Recycling, Université Libre de Bruxelles, 50 Avenue FD Roosevelt, CP194/03, 1050 Brussels, Belgium. Contact e-mail: sgodet@ulb.ac.be MATTEO CARUSO and JEAN-LOUIS COLLET are with the CRM Group, Avenue du Bois Saint Jean 21 P59, 4000 Liège, Belgium.

Manuscript submitted November 21, 2018.
Article published online May 21, 2019

Table I. Chemical Compositions (in Weight Percent) of the Investigated Steels. Ac_1 and Ac_3 Temperatures Were Calculated Using Equations from Reference [34] and B_s and M_s from Reference [33]

Steel	C	Si	Mn	Cr	P	S	N	Fe	Ac_1	Ac_3	B_s	M_s
0.4Si	0.2	0.4	2.4	0.2	0.003	0.002	0.005	balance	985 K (712 °C)	1075 K (802 °C)	819 K (546 °C)	652 K (379 °C)
0.8Si	0.2	0.8	2.3	0.2	0.003	0.003	0.007	balance	998 K (725 °C)	1124 K (851 °C)	819 K (546 °C)	649 K (376 °C)
1.5Si	0.2	1.5	2.3	0.2	0.003	0.002	0.005	balance	1018 K (745 °C)	1125 K (852 °C)	803 K (530 °C)	640 K (367 °C)

as well as results from our previous studies, have shown that carbide precipitation and austenite decomposition take place during the Q&P process despite relatively high-silicon additions, *i.e.,* 1.5 wt pct.[18–21] Furthermore, our previous *in situ* synchrotron investigation[22] on a 0.2C-1.5Si-2.3Mn-0.2Cr steel showed that almost 50 pct of the total amount of carbon remains trapped in the BCC phases (*i.e.,* tempered martensite and bainite) and does not contribute to the austenite stabilization process. Nevertheless, using appropriate Q&P process parameters, more than 10 pct of austenite was successfully retained at room temperature. Similar trends were reported elsewhere.[23] Several heat treatments leading to an effective stabilization of austenite in low-silicon steels have also been reported. Such is the case for intercritically annealed 0.2C-3.5Mn-0.45Si-0.22Al steels where 10 pct of austenite was measured after Q&P,[24] or after anisothermal partitioning[25] or one-step partitioning of a 0.16C-1.1Mn-0.5Si.[26] Thus, the fact that silicon prevents the formation of carbon sinks in the martensite matrix cannot solely explain its stabilization effect on the retained austenite.

Another effect of silicon is related to the decomposition of austenite. Kim *et al.*[27] have shown that additions of silicon in a 1.0C-1Mn delay the austenite decomposition during the partitioning step. Similar observations have been reported for TRIP steels,[28] bearing steels,[29] and one-step Q&P steels.[30] This effect is of significant importance, especially when considering commercial low-alloyed Q&P steels. Large fractions of bainite can be formed during the partitioning step, limiting the amount of retained austenite at room temperature.[21] For instance, the bainite transformation taking place during a 1-hour partitioning step in a 0.2C-0.8Si-2.2Mn-0.8Cr steel leads to negligible amounts of retained austenite.[31] Similar results were reported for a 0.35C-1.3Mn-0.74Si, where the retained austenite phase fraction tends to decrease with the increasing partitioning time due to the bainite transformation.[32]

The current study presents a comparative study to assess the effect of silicon content on the microstructural evolution during an industrial Q&P cycle in a 0.2C-2.3Mn commercial grade. Three different silicon contents are investigated (*i.e.,* 0.4, 0.8, and 1.5 Si wt pct). *In situ* HEXRD coupled with very high acquisition rates are used to monitor the quantitative evolution of phase fractions during the entire Q&P treatment.

II. EXPERIMENTAL PROCEDURES

The Q&P heat treatments were performed on three steel grades exhibiting identical chemical compositions with the exception of the silicon content, which varies from 0.4 to 1.5 wt pct. Table I summarizes the investigated compositions, along with the corresponding characteristic temperatures Ac_1, Ac_3, B_s, and M_s calculated according to the equations given in References 33 and 34.

The applied Q&P heat treatment is represented in Figure 1. Samples were first heated up to 1173 K (900 °C) at 10 K/s and held for 300 seconds in order to obtain a fully austenitic microstructure. They were then quenched at 50 K/s to a targeted initial quench temperature Q_T of 593 K (320 °C). This temperature corresponds to the maximum retained austenite phase fraction at room temperature for the 1.5Si alloy.[21,22] The experimental Q_T temperatures were 585 K, 584 K, and 578 K (312 °C, 311 °C, and 305 °C) for the 0.4Si, 0.8Si, and 1.5Si alloys, respectively. Taking into account an accuracy of ± 5 K on Q_T during cooling, the achieved Q_T is assumed to be the same for the 3 steel grades. After initial quenching, the samples were heated up at 10 K/s to the partitioning temperature of 673 K (400 °C) for 120 seconds, then quenched to room temperature at 50 K/s.

In situ experiments were carried out on the high-resolution ID11 beam line of the European Synchrotron Radiation Facility (ESRF, Grenoble, France). The high-energy monochromatic beam (E = 65 keV, λ = 0.19 Å) allowed to work in transmission diffraction mode, such that the X-ray beam probes all the grains through the thickness. High-resolution patterns were obtained using a beam size of 0.2 × 0.2 mm^2, and a total volume of 0.06 mm^3 was analyzed. This volume is considered statistically relevant since the prior austenite grain size is about 15 μm. The high acquisition rate (*i.e.,* 5 Hz) of the FReLoN CCD camera allowed a precise follow-up of the evolution of the diffraction peaks during the Q&P treatment. The 2D-diffraction rings were reduced to the 1D profile (intensity—2θ) using the Fit2D program developed at ESRF.[35] The volume fraction and lattice parameters were extracted from the integrated intensities and the scattering angles of three face-centered cubic peaks ($\{200\}_\gamma$, $\{220\}_\gamma$, and $\{311\}_\gamma$) and three body-centered cubic peaks ($\{200\}_\alpha$, $\{211\}_\alpha$, and $\{220\}_\alpha$).[5] The absolute error made on phase fractions was estimated to be 1 pct. The carbon contents are expressed in wt pct, and the uncertainties are about 0.015 pct.[36]

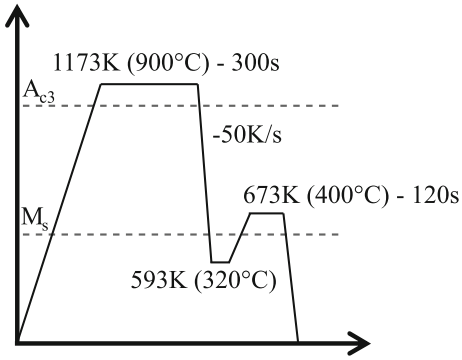

Fig. 1—Schematic representation of the investigated quenching and partitioning (Q&P) heat treatment.

The heat treatments were conducted on an Instron electrothermal mechanical testing (ETMT) heating stage. Samples were heated up by Joule effect and the cooling process involved heat extraction through the device jaws. The high soaking temperature at 1173 K (900 °C) was performed under controlled atmosphere using argon. The temperature was monitored using a Pt/Pt-13 pct Rh thermocouple spot-welded to the sample. Special attention was paid to characterize the material in the vicinity of the welded thermocouple. After *in situ* experiments, samples were prepared for metallographic investigations using conventional methods.[21]

III. RESULTS

A. *In Situ Synchrotron Characterization*

1. *First Quench*

Austenite decomposition during the first quench occurs in two steps (Figure 2): minor amounts of austenite transforms into BCC phase above M_s, between 873 K and 673 K (600 °C and 400 °C), while the main martensitic transformation occurs below M_s, *i.e.,* 653 K (380 °C).

The amount of transformed austenite above M_s depends on the silicon content: BCC-phase volume fractions of 25.9 pct, 13.1 pct, and 5 pct are measured at 673 K (400 °C) for the 0.4Si, 0.8Si, and 1.5Si alloys, respectively. The small BCC fraction measured in the 1.5Si steel grade results from the formation of a ferritic layer of approximately 15 μm on the specimen surface. This is related to the lack of hardenability following surface decarburization inherited from the preceding industrial processing of the steel sheet.[37,38] On the contrary, the austenite decomposition in the 0.4Si and 0.8Si grades is likely to occur also in the bulk of the specimen, because the decarburization phenomenon cannot solely explain how such high fractions of BCC formed.

Below a temperature of about 643 K (370 °C), martensitic transformation takes place, and a significant decrease of the FCC-phase fractions occurs. At the end of the initial quench, the 0.4Si, 0.8Si, and 1.5Si alloys exhibit total BCC volume fractions of 71.7, 72.6, and 78.4 pct, respectively. The precise fractions of martensite formed are retrieved by subtracting the fractions formed above M_s from the total BCC fraction. Thus, at the end of the first quench, the martensite phase fractions are 45.8, 59.5, and 73.1 pct for the 0.4Si, 0.8Si, and 1.5Si, respectively. The small deviations in the quenching temperatures alone are unlikely to be responsible for these variations in martensite fraction, which appear to be mainly related to the silicon content.

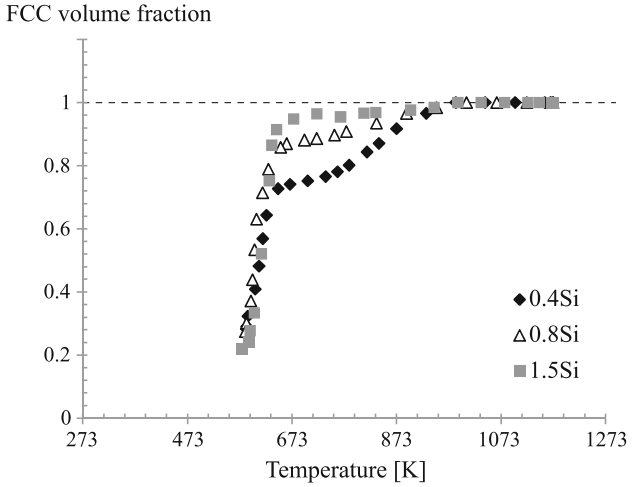

Fig. 2—Evolution of FCC volume fraction with temperature during the initial quench to Q_T.

The evolution of the austenite lattice parameter a_γ with temperature during the initial quench is plotted in Figure 3 for the three steel grades. Despite the formation of a considerable amount of BCC phase above M_s, between 873 K and 673 K (600 °C and 400 °C) in the 0.4Si and 0.8Si grades, the evolution of their austenite lattice parameter remains linear until the martensitic transformation occurs. Assuming the absence of mechanical and chemical contributions to the evolution of the austenite lattice parameter, the average constant thermal expansion coefficient of the FCC phase between 1173 K and 673 K (900 °C and 400 °C) is 2.3493×10^{-5} K^{-1}. This thermal expansion coefficient is in good agreement with the ones reported by Lu *et al.*[39] and Allain *et al.*[36]

2. *Reheating*

During the reheating step from Q_T up to the partitioning temperature P_T = 673 K (400 °C), the evolution of the BCC lattice parameter is purely linear (Figure 4(a)). On the other hand, the austenite lattice parameter first evolves linearly, then, at $T > 623$ K (350 °C), deviates from a purely thermal expansion behavior (Figure 4(b), dashed lines). It is interesting to notice that the deviation from linearity at 673 K (400 °C) increases as the silicon content increases.

A decrease in austenite fraction is observed during the reheating step for all investigated grades (Figure 5). The extent of this decrease is also influenced by the silicon content: in the temperature range from Q_T to P_T = 673 K (400 °C), 7.8, 5.7 and 5.0 pct of austenite (in terms of absolute fractions) is consumed in the 0.4Si, 0.8Si, and 1.5Si steel grades, respectively.

3. *Partitioning*

The intensities of the $\{200\}_\gamma$ and $\{220\}_\gamma$ austenite peaks decrease during partitioning, and their positions shift toward lower 2θ angles (Figure 6). The silicon content has an evident impact on these evolutions.

The decreasing intensity of the austenite peaks implies a decrease of the volume fraction of austenite during the partitioning step (Figure 7). This is due to the bainite transformation that takes place during partitioning. From Figures 6 and 7, it appears clearly that the fraction of austenite transformed into bainite increases as the silicon content decreases. For the 0.4Si grade, almost the entire residual austenite transforms into bainite within 120 seconds of partitioning at 400 °C.

Furthermore, the change in position of the austenite peaks implies a change in lattice parameter (Figure 8). There is an almost continuous increase in the austenite lattice parameter with time during the partitioning, regardless of the silicon content. While the 0.8Si and 1.5Si grades exhibit a similar increase in a_γ, the expansion of the austenite lattice is significantly lower in the 0.4Si steel grade. However, it must be noted that there are large experimental errors associated with the

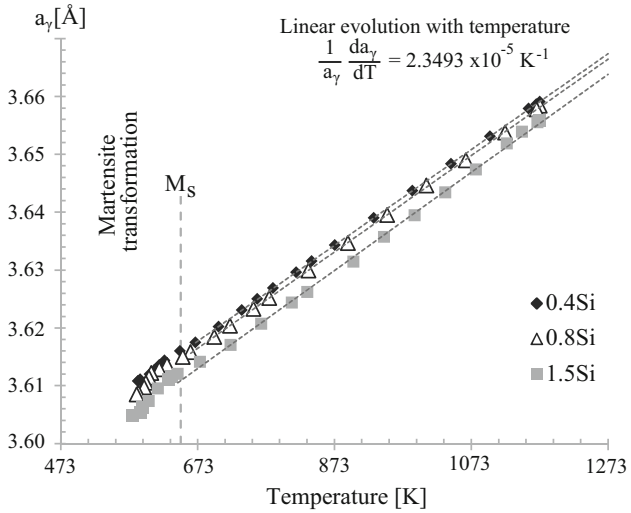

Fig. 3—Evolution of the austenite lattice parameter with temperature during the initial quench. The thermal expansion parameter of austenite is measured from the data recorded during the initial quench (1173 K to 673 K (900 °C to 400 °C)).

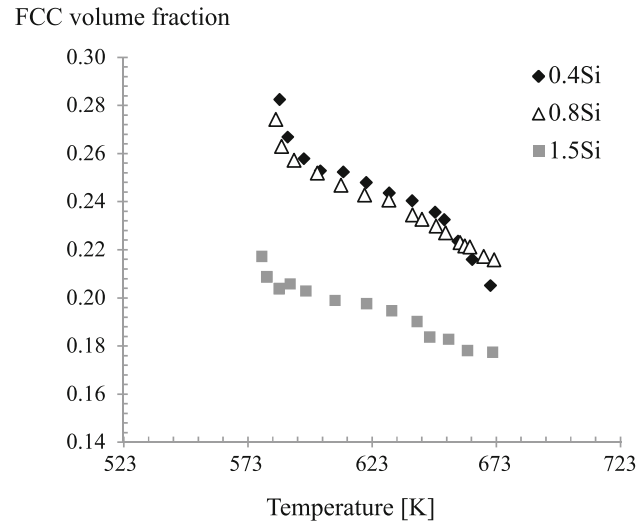

Fig. 5—Evolution of the FCC volume fraction during the reheating stage from Q_T to 673K (400 °C).

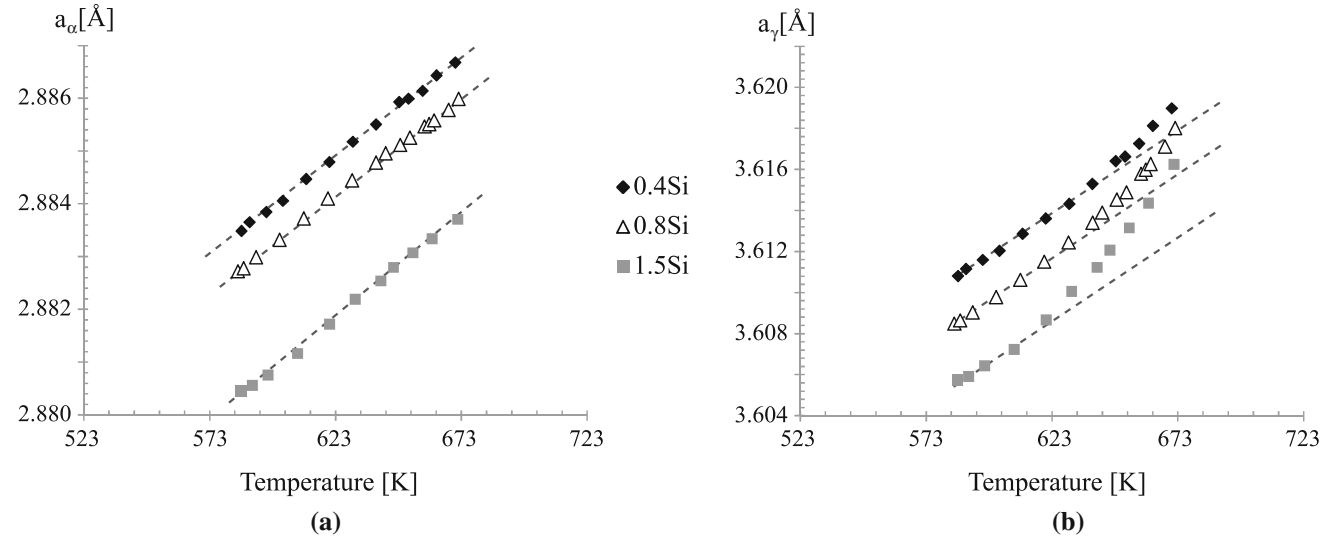

Fig. 4—Evolution of (*a*) the BCC and (*b*) the FCC lattice parameters during the reheating stage from Q_T to 673 K (400 °C).

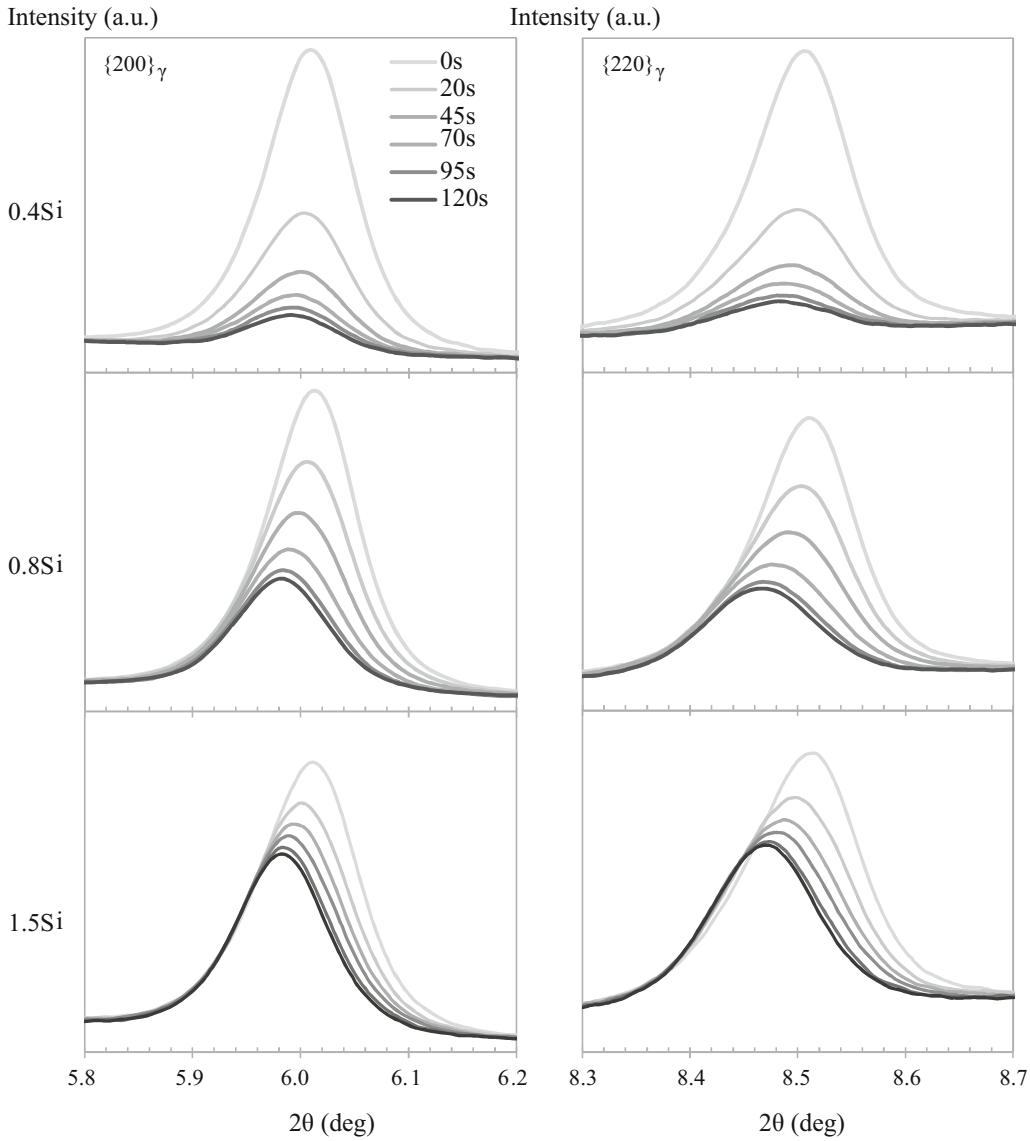

Fig. 6—1D diffractograms of the {200}γ and {220}γ FCC peaks after different partitioning times at 673 K (400 °C).

determination of the austenite lattice parameter when the phase fraction is less than 3 pct (as in the 0.4Si after long partitioning times).

4. *Final Quench*

The intensities of austenite peaks do not change significantly during the final cooling step to room temperature, for all three steel grades. At the end of the partitioning step, the measured FCC fraction was 1.6, 7.1, and 11.0 pct for the 0.4Si, 0.8Si, and 1.5Si, respectively, and 1.5, 7.1, and 10.9 pct after the final quench.

At room temperature, minor isolated diffraction peaks can be recognized at about $2\theta = 7.1°$ (Figure 9), especially in the 0.8Si and 0.4Si steel grades. This is likely related to the important carbide precipitation occurring in these grades. However, due to the low signal-to-noise ratio, the phase identification or phase quantification of these potential carbides is not possible.

B. *Microstructural Characterization*

Table II summarizes the volume fractions of the phases formed during the Q&P heat treatment for the three steel grades, along with the amount of carbon in austenite determined using the relationship developed by Toji *et al.*[40] The total amount of carbon that has not partitioned (*i.e.,* trapped in BCC phases and in carbides) is also reported, and is determined by subtracting the fraction of carbon contained within the austenite from the nominal carbon content (*i.e.,* 0.2 wt pct).

EBSD quality maps of the three final Q&P microstructures at room temperature are shown in Figure 10, where the red zones correspond to retained austenite grains. The amount of retained austenite clearly decreases with the decreasing silicon content. SEM observations (Figure 11) show that carbide precipitation occurred in the three investigated materials, albeit the carbide density increases with the decreasing

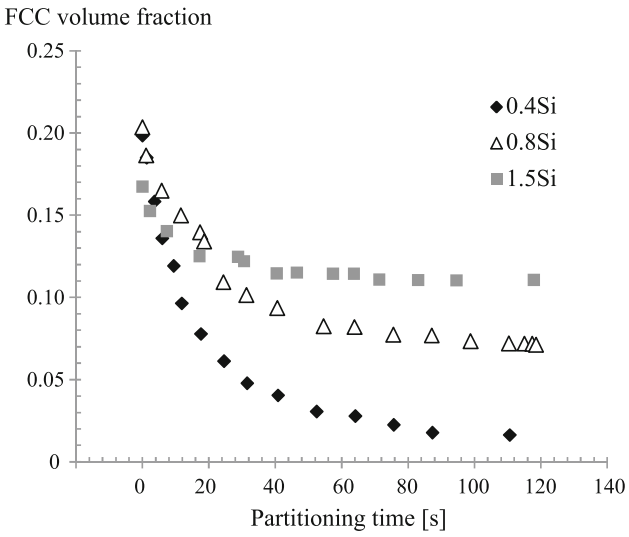

Fig. 7—Evolution of the FCC volume fraction during the partitioning step at 673 K (400 °C).

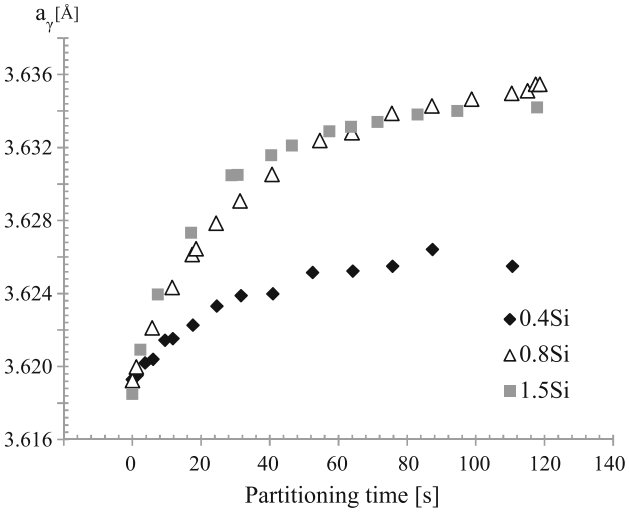

Fig. 8—Evolution of the FCC lattice parameters during the partitioning step at 673 K (400 °C).

silicon content. Thus, despite the presence of 1.5 wt pct of silicon, carbides are still detected in martensite laths as it can be seen in the SEM micrograph (Figure 11), which is consistent with our previous study.[21]

IV. DISCUSSION

The current results show that the silicon content has a first impact on the microstructural evolution during the first quench. Austenite decomposes into a BCC phase between ~ 873 K and ~ 673 K (~ 600 °C and ~ 400 °C), *i.e.,* below Ac_1 but above M_s (Figure 2). The magnitude of this transformation increases with the decreasing silicon contents. Based on the observed transformation temperature range, the resulting BCC phase can only be identified as bainite. This is confirmed by the fact that no ferrite was observed in the microstructures, with the exception of a small decarburization layer on the surfaces of the samples. Such effect of silicon on the bainite transformation during cooling has already been reported in the literature.[41] It should be pointed out that no carbon diffusion is observed between the bainite and the austenite during the first quench, as shown by the linear evolution of the austenite lattice parameter in this temperature range. This can be due to the fast cooling rate, which would prevent such diffusion to take place, or to carbide precipitation in the newly formed bainite. In any case, the total amount of BCC phases at the end of the first quench (*i.e.,* bainite and martensite) is similar regardless of the silicon content. Thus, it can be reasonably assumed that the subsequent microstructural evolution during reheating and partitioning is not significantly influenced by the transformations occurring prior to M_s.

Additions of silicon improve significantly austenite retention during the quench and partitioning treatment. More specifically, if 11 pct of retained austenite could be stabilized in the 1.5Si grade, only 7 pct of retained austenite is present in the 0.8Si grade while the 0.4Si grade contains almost no retained austenite (Table II).

Our previous study on the 1.5Si steel [22] has demonstrated that two phenomena are responsible for the stabilization of austenite during the partitioning of a commercial Q&P grades: carbon partitioning from martensite, and carbon rejection from the isothermal bainite transformation. However, the relative contribution of these two mechanisms cannot be estimated due to their close and mutual interaction. For instance, carbon partitioning from martensite enriches austenite, which in turn slows down the isothermal bainite transformation. It appears clearly that the silicon content has an effect on both mechanisms.

First, silicon seems to effectively suppress, at least partially, carbide precipitation in the BCC phases. Although some carbides are observed in the BCC phases, regardless of the silicon content, more carbides are clearly observed in the lower silicon grades. The exact carbide-phase fraction cannot be measured, and it is impossible to determine whether these carbides precipitate primarily in martensite or in bainite. Given the martensite fraction in the current Q&P microstructure, it is reasonable to assume that a significant fraction of them have precipitated in the martensite matrix. In such case, less carbon would be available for partitioning from martensite to austenite.

Second, silicon has a pronounced effect on the austenite decomposition into bainite during the reheating and partitioning steps, since larger fractions of bainite are being formed when the silicon content is lower (Table II). The silicon content is known to affect the isothermal bainite transformation kinetics, and the subsequent carbon rejection from the bainite to the austenite. According to Quidort and Bréchet[42,43] and assuming that no carbide precipitation occurs, the bainite transformation is limited by the diffusion of carbon atoms from the bainite growing tip into the austenite. More specifically, the kinetically limiting step

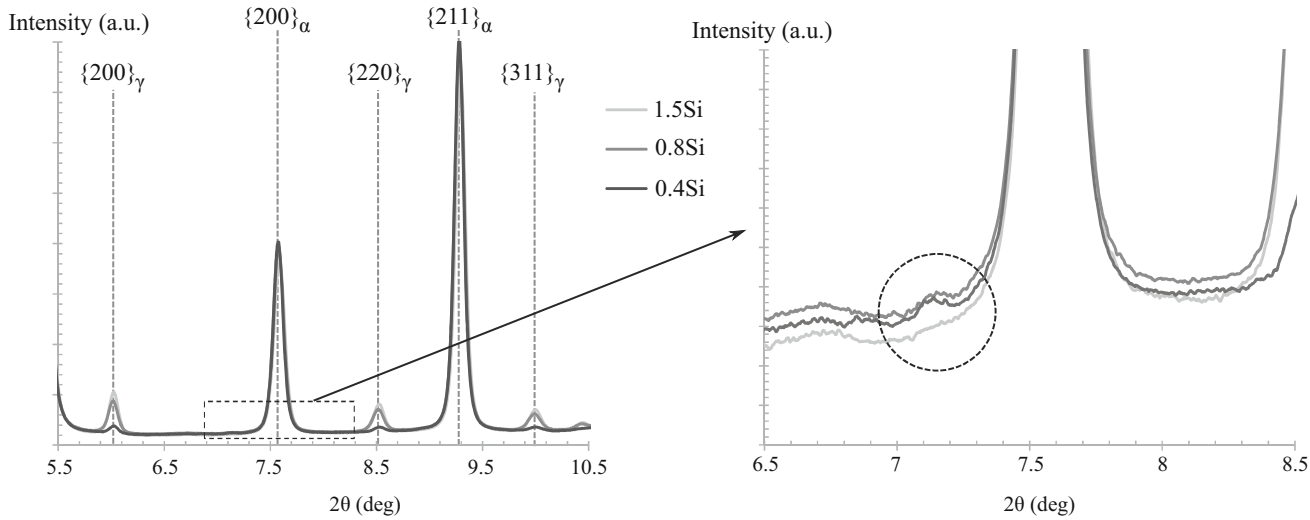

Fig. 9—1D diffractograms of the final Q&P specimens: (left) for 2θ between 5.5 and 10.5, (right) close-up view for 2θ between 6.5 and 8.5. The dotted circle could correspond to possible carbide diffraction peaks.

Table II. Volume Fractions of Phases Formed During Q&P for the Three Steel Grades, Along with the Amount of Carbon Partitioned and Non-partitioned at the End of the Heat Treatment

	BCC Initial Quench (> M_s)	Martensite (< M_s)	BCC Reheat	BCC Partition	RA_{final}	C_{RA} (Weight Percent)	C Trapped in BCC and Carbides (Weight Percent)
0.4Si	25.9	45.8	7.8	19.0	1.5	–	0.20
0.8Si	13.1	59.5	5.7	14.6	7.1	0.79	0.14
1.5Si	5.3	73.1	5.0	5.7	10.9	0.83	0.09

The error made on the phase volume fraction measurement is ± 1 pct in terms of absolute phase fraction.

is the diffusion of carbon in austenite far from the bainite/austenite interface. The resulting carbon enrichment progressively stabilizes the austenite until the bainite transformation is stopped. If carbides precipitate in bainite close to the bainite/austenite interface, the local carbon concentration decreases such that less carbon can diffuse to austenite, limiting its stabilization. Thus, carbide precipitation leads to a faster bainite transformation kinetics, and to a higher bainite fraction in the final microstructure. This was proved experimentally by Jacques *et al.* in their study of the effect of the silicon content on the stabilization of austenite in TRIP steels,[28] and is in good agreement with the current results. Particularly, it is interesting to notice that in the current study, the austenite carbon contents are nearly the same in the 0.8Si and 1.5Si grades, *i.e.,* 0.79 wt pct and 0.83 wt pct, respectively. This critical carbon content appears to inhibit further austenite decomposition into bainite at 673 K (400 °C) in the investigated steel grades.

To summarize, a lower silicon content leads to carbide precipitation, which in turn leads to a decrease in the austenite stability due to (i) less carbon available for partitioning from the martensite, and (ii) faster bainite transformation kinetics and less carbon rejection from the growing bainitic tip. Unfortunately, it is impossible to determine the relative contributions of each mechanism, because this would require a precise knowledge of the amount of carbon trapped in the BCC phases. It is, however, likely that both mechanisms are heavily influenced by the carbide precipitation, which is turn impacted by the silicon content. Almost no austenite is stabilized during the partitioning step in the 0.4Si grade, implying that both carbon partitioning from martensite and the carbon rejection during bainite transformation did not occur.

The current results underline the importance of the bainite transformation in commercial Q&P grades. While silicon is usually added in order to maximize carbon partitioning from the martensite, a second significant effect of silicon is to impede the bainite transformation during partitioning, which plays a key role in the stabilization of austenite. As shown here, austenite is progressively consumed by bainite until a critical carbon content of ~ 0.8 wt pct is reached. When the silicon content is low enough, *i.e.,* 0.4 wt pct in the current study, this critical content is never reached due to the extensive carbide precipitation. The final retained austenite fraction is thus determined by the kinetics of bainite transformation during partitioning. It follows that additions of elements such as Cr or Mo to the low-silicon grades could be considered in

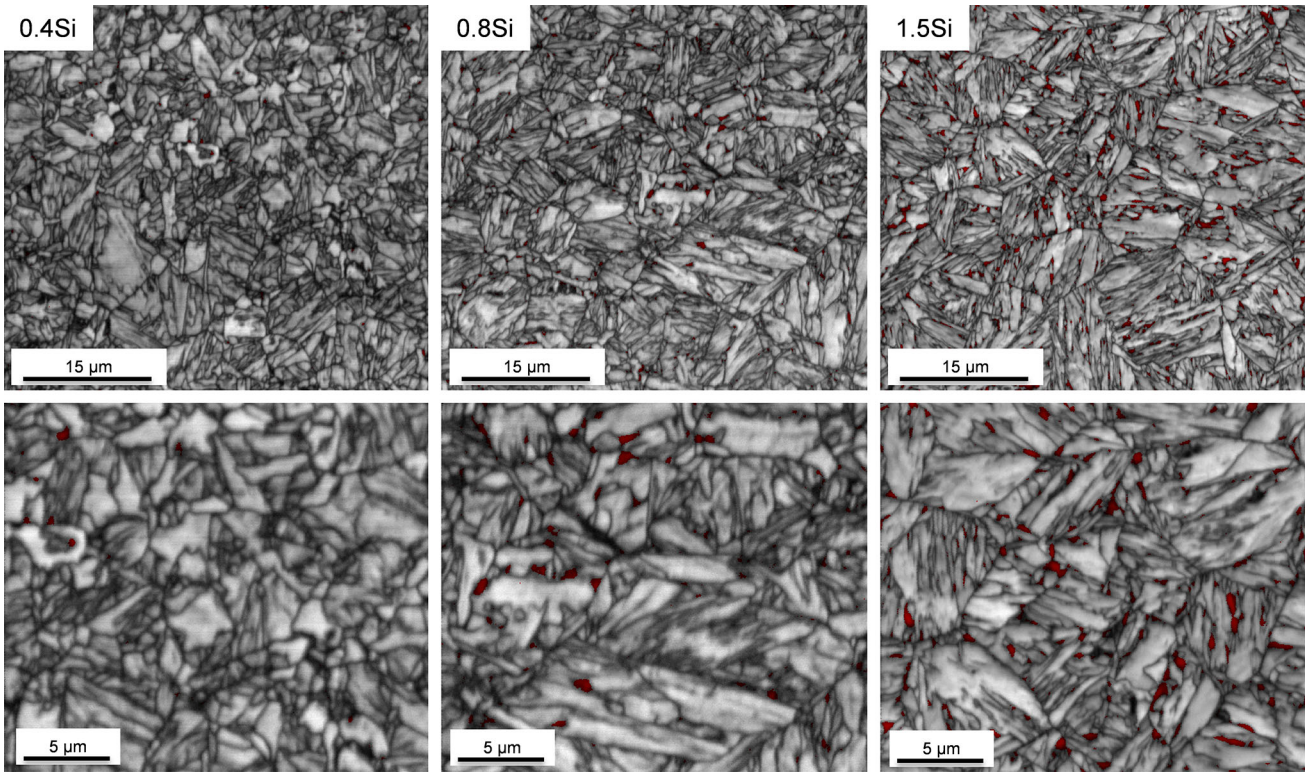

Fig. 10—EBSD micrographs of the three final Q&P microstructures showing combined Image Quality and Austenite phase (in red) maps. Magnification of 2000× and 4000× are presented in the first and the second rows, respectively (Color figure online).

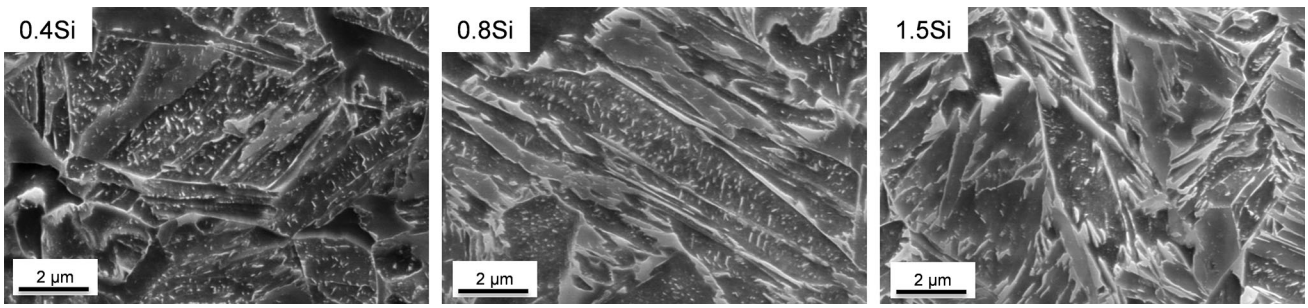

Fig. 11—SEM micrographs the final Q&P microstructures showing carbide precipitation.

order to avoid the decomposition of austenite during the Q&P process.

V. CONCLUSIONS

The current study demonstrates the key role of silicon in Q&P steels. The fraction of retained austenite obtained following the same Q&P treatment decreases as the silicon content decreases. The carbon content of the retained austenite (~ 0.8 pct wt) is similar for both the 1.5Si and 0.8Si grades. The retained austenite fraction obtained in the 0.4Si grade is negligible. Silicon promotes the two mechanisms responsible for the carbon enrichment of austenite in Q&P steels:

(i) It reduces (partially) the carbide precipitation in martensite, making more carbon available for partitioning to austenite.
(ii) It suppresses the carbide precipitation at the bainite/austenite interface, which in turn inhibits the austenite decomposition into bainite that takes place during partitioning.

The impact of silicon on the bainite transformation, which determines the final amount of retained austenite, is particularly important in commercial low-alloyed Q&P grades. In order to improve austenite retention in low-silicon steel grades, additions of others bainite retarding elements, such as Cr or Mo, could be considered to avoid austenite decomposition during the partitioning step.

ACKNOWLEDGMENTS

We thank the European Synchrotron Radiation Facility for the provision of synchrotron radiation facilities and would also like to thank P. Sedmak and T. Buslaps for assistance in using beamline ID11.

REFERENCES

1. J. Speer, D.K. Matlock, B.C. De Cooman, and J.G. Schroth: *Acta Mater.*, 2003, vol. 51, pp. 2611–22.
2. J.G. Speer, D.V. Edmonds, F.C. Rizzo, and D.K. Matlock: *Curr. Opin. Solid State Mater. Sci.*, 2004, vol. 8, pp. 219–37.
3. M.J. Santofimia, L. Zhao, R. Petrov, C. Kwakernaak, W.G. Sloof, and J. Sietsma: *Acta Mater.*, 2011, vol. 59, pp. 6059–68.
4. D. De Knijf, C. Föjer, L.A.I. Kestens, and R. Petrov: *Mater. Sci. Eng. A*, 2015, vol. 638, pp. 219–27.
5. N.H. Van Dijk, A.M. Butt, L. Zhao, J. Sietsma, S.E. Offerman, J.P. Wright, and S. Van Der Zwaag: *Acta Mater.*, 2005, vol. 53, pp. 5439–47.
6. X.C. Xiong, B. Chen, M.X. Huang, J.F. Wang, and L. Wang: *Scr. Mater.*, 2013, vol. 68, pp. 321–24.
7. P.J. Jacques, F. Delannay, and J. Ladrière: *Metall. Mater. Trans. A Phys.*, 2001, vol. 32A, pp. 2759–68.
8. H.S. Zhao, W. Li, X. Zhu, X.H. Lu, L. Wang, S. Zhou, and X.J. Jin: *Mater. Sci. Eng. A*, 2016, vol. 649, pp. 18–26.
9. L. Samek, E. De Moor, J. Penning, and B.C. De Cooman: *Metall. Mater. Trans. A*, 2006, vol. 37A, pp. 109–24.
10. J.G. Speer, A.M. Streicher, D.K. Matlock, F. Rizzo, and G. Krauss: *Austenite formation and decomposition*, TMS, Warrendale, Pa, Chicago, 2003, pp. 505–22.
11. E. Girault, A. Mertens, P. Jacques, Y. Houbaert, B. Verlinden, and J. Van Humbeeck: *Scr. Mater.*, 2001, vol. 44, pp. 885–92.
12. H.K.D.H. Bhadeshia and D.V. Edmonds: *Metall. Trans. A*, 1979, vol. 10, pp. 895–907.
13. M. Takahashi and H.K.D.H. Bhadeshia: *Mater. Trans. JIM*, 1991, vol. 32, pp. 689–96.
14. E. Kozeschnik and H.K.D.H. Bhadeshia: *Mater. Sci. Technol.*, 2008, vol. 24, pp. 343–47.
15. A.J. Clarke, J.G. Speer, M.K. Miller, R.E. Hackenberg, D.V. Edmonds, D.K. Matlock, F.C. Rizzo, K.D. Clarke, and E. De Moor: *Acta Mater.*, 2008, vol. 56, pp. 16–22.
16. J. Tobata, K.-L. Ngo-Huynh, N. Nakada, T. Tsuchiyama, and S. Takaki: *ISIJ Int.*, 2012, vol. 52, pp. 1377–82.
17. P.J. Jacques, E. Girault, A. Mertens, B. Verlinden, J. Van Humbeeck, and F. Delannay: *ISIJ Int.*, 2001, vol. 41, pp. 1068–74.
18. Y. Toji, G. Miyamoto, and D. Raabe: *Acta Mater.*, 2015, vol. 86, pp. 137–47.
19. D.T. Pierce, D.R. Coughlin, D.L. Williamson, K.D. Clarke, A.J. Clarke, J.G. Speer, and E. De Moor: *Acta Mater.*, 2014, vol. 90, pp. 417–30.
20. F. HajyAkbary, J. Sietsma, G. Miyamoto, T. Furuhara, and M.J. Santofimia: *Acta Mater.*, 2016, vol. 104, pp. 72–83.
21. P. Huyghe, L. Malet, M. Caruso, C. Georges, and S. Godet: *Mater. Sci. Eng. A*, 2017, vol. 701, pp. 254–63.
22. P. Huyghe, M. Caruso, J.L. Collet, S. Dépinoy, and S. Godet: *Mater. Sci. Eng. A*, 2019, vol. 743, pp. 175–84.
23. S. Allain, G. Geandier, J.-C. Hell, M. Soler, F. Danoix, and M. Gouné: *Metals*, 2017, vol. 7, art. no. 232.
24. M.J. Santofimia, T. Nguyen-Minh, L. Zhao, R. Petrov, I. Sabirov, and J. Sietsma: *Mater. Sci. Eng. A*, 2010, vol. 527, pp. 6429–39.
25. G.K. Bansal, V. Rajinikanth, C. Ghosh, V.C. Srivastava, S. Kundu, and S.G. Chowdhury: *Metall. Mater. Trans. A*, 2018, vol. 49A, pp. 3501–14.
26. G.K. Bansal, M. Pradeep, C. Ghosh, V. Rajinikanth, V.C. Srivastava, A.N. Bhagat, and S. Kundu: *Metall. Mater. Trans. A*, 2019, vol. 50A, pp. 547–55.
27. B. Kim, J. Sietsma, and M.J. Santofimia: *Mater. Des.*, 2017, vol. 127, pp. 336–45.
28. P. Jacques, E. Girault, T. Catlin, N. Geerlofs, T. Kop, S. van der Zwaag, and F. Delannay: *Mater. Sci. Eng. A*, 1999, vols. 273–275, pp. 475–79.
29. T. Sourmail and M. Millot-Méheux: *Mater. Sci. Technol. U.K.*, 2016, vol. 32, pp. 1126–32.
30. D.H. Kim, J.G. Speer, H.S. Kim, and B.C. De Cooman: *Metall. Mater. Trans. A*, 2009, vol. 40A, pp. 2048–60.
31. W.T. Zhao, X.F. Huang, and W.G. Huang: *Mater. Sci. Technol.*, 2016, vol. 32, pp. 1374–81.
32. D.K. Matlock, V.E. Bräutigam, and J.G. Speer: *Mater. Sci. Forum*, 2003, vols. 426–432, pp. 1089–94.
33. S.M.C. van Bohemen: *Mater. Sci. Technol.*, 2012, vol. 28, pp. 487–95.
34. K.W. Andrews: *J. Iron Steel Inst.*, 1965, vol. 203, pp. 721–29.
35. ESRF Fit2D, http://www.esrf.eu/computing/scientific/FIT2D/. Accessed 20 November 2018.
36. S.Y.P. Allain, G. Geandier, J.C. Hell, M. Soler, F. Danoix, and M. Gouné, *Scr. Mater.*, 2017, vol. 131, pp. 15–18.
37. J. Epp, T. Hirsch, and C. Curfs: *Metall. Mater. Trans. A*, 2012, vol. 43A, pp. 2210–17.
38. J. Epp, H. Surm, O. Kessler, and T. Hirsch: *Acta Mater.*, 2007, vol. 55, pp. 5959–67.
39. X.G. Lu, M. Selleby, and B. Sundman: *Acta Mater.*, 2005, vol. 53, pp. 2259–72.
40. Y. Toji, H. Matsuda, M. Herbig, P.-P. Choi, and D. Raabe: *Acta Mater.*, 2014, vol. 65, pp. 215–28.
41. J. Drumond, O. Girina, J.F. de Siva Filho, N. Fonstein, and C.A.S. de Oliveira: *Metallogr. Microstruct. Anal.*, 2012, vol. 1, pp. 217–23.
42. D. Quidort and Y.J.M. Brechet: *Acta Mater.*, 2001, vol. 49, pp. 4161–70.
43. D. Quidort and Y. Bréchet: *Scr. Mater.*, 2002, vol. 47, pp. 151–56.